

Control of ecological outcomes through deliberate parameter changes in a model of the gut microbiome

Zipeng Wang,¹ Eric W. Jones,^{1,*} Joshua M. Mueller,^{1,2} and Jean M. Carlson^{1,2}

¹*Department of Physics, University of California, Santa Barbara, Santa Barbara, California, USA*

²*Interdepartmental Graduate Program in Dynamical Neuroscience,
University of California, Santa Barbara, Santa Barbara, California, USA*

(Dated: May 28, 2022)

The generalized Lotka-Volterra (gLV) equations are a mathematical proxy for ecological dynamics. We focus on a gLV model of the gut microbiome, in which the evolution of the gut microbial state is determined in part by pairwise inter-species interaction parameters that encode environmentally-mediated resource competition between microbes. We develop an *in silico* method that controls the steady-state outcome of the system by adjusting these interaction parameters. This approach is confined to a bistable region of the gLV model. In this method, a dimensionality reduction technique called steady-state reduction (SSR) is first used to generate a two-dimensional (2D) gLV model that approximates the high-dimensional dynamics on the 2D subspace spanned by the two steady states. Then a bifurcation analysis of the 2D model analytically determines parameter modifications that drive an initial condition to a target steady state. This parameter modification of the reduced 2D model guides parameter modifications of the original high-dimensional model, resulting in a change of steady-state outcome in the high-dimensional model. This control method, called SPARC (SSR-guided parameter change), bypasses the computational challenge of directly determining parameter modifications in the original high-dimensional system. SPARC could guide the development of indirect bacteriotherapies, which seek to change microbial compositions by deliberately modifying gut environmental variables such as gut acidity or macronutrient availability.

I. INTRODUCTION

A shared goal in environmental management, ecology, and medicine is to drive an ecosystem towards a target community structure. For example, ocean and lake ecosystems benefit from the suppression of algal blooms, the control of invasive fish species helps preserve the biodiversity of local fish populations, and certain microbial compositions of the gut microbiome that resist pathogenic infections improve the health of the host [1–3]. It is common to control these ecosystems by directly altering the ecological composition of the community: unwanted algae can be removed by clay, invasive fish species can be killed by biocides, and gut pathogens can be killed by antibiotics [1, 4, 5].

In contrast to these direct methods that modify the ecological state of the system, *indirect* methods can control ecological outcomes by modifying environmental variables which effectively change the dynamical landscape of the system [6]. For example, indirect control methods commonly applied to the previously mentioned systems include reducing nutrient concentrations in water to inhibit algal blooms, lowering the water level to disrupt the spawning of invasive fish, and introducing prebiotics to promote biodiversity in the gut microbiome [1, 7, 8].

In this paper, we create an *in silico* technique that drives an ecological model towards a target outcome by manipulating parameters that correspond to coarse-grained interactions between populations. Specifically,

we seek a finite-time modification of the dynamical landscape that drives an arbitrary initial condition towards a target state. Although the intervention is temporary, the change in the ecological outcome can be permanent.

This control method is demonstrated in the context of a data-driven model of the gut microbiome [9]. Ecological dynamics are simulated using the generalized Lotka-Volterra (gLV) equations, a commonly used model in theoretical ecology [10]. In these equations, species-species interaction parameters represent environmentally-mediated competition for resources. These systems are often modeled by high-dimensional gLV equations in order to capture the dynamics of the large number of microbial species that inhabit the gut microbiome. In these models, the many inter-species feedbacks lead to complex dynamics. Accordingly, it is difficult to achieve a target steady-state outcome by naively modifying parameter values, as such an approach requires exhaustively searching a large parameter space.

To address these challenges, we focus on a bistable region of the ecological phase space that includes one target steady state and another alternative steady state within the gLV system. Then, a dimensionality-reduction technique called steady-state reduction (SSR) is used to approximate the bistable region of interest and to create a low-dimensional system with a compressed set of interaction parameters [11]. A bifurcation analysis of this 2D system determines a parameter modification that produces a targeted change in steady-state outcome. Lastly, the low-dimensional interaction parameter change is associated with a parameter change in the high-dimensional model, which drives the original system to the target

* ewj@physics.ucsb.edu

state.

This control method, referred to as SPARC (SSR-guided parameter change), is applied to an 11-dimensional gLV model fit to time-series data from a mouse microbiome experiment [3, 9]. In this experimentally-derived gLV model, SPARC successfully alters the steady-state outcomes of initial conditions by modifying interaction parameters of the model. SPARC as an *in silico* approach is effective when applied to generic gLV systems, but its applicability to real-world systems is dependent on the fidelity of the underlying gLV model. More generally, this method offers a systematic understanding of how environmental factors and species-species interactions can be manipulated to control ecological outcomes.

II. MATERIALS AND METHODS

A. Generalized Lotka-Volterra equations

The generalized Lotka-Volterra (gLV) equations are a traditional model in theoretical ecology. Due to their flexibility, gLV models have been used to describe a wide variety of system dynamics, including the market values of firms in the stock market, wolf predation of multiple prey species, and the infection dynamics of RNA viruses [12–14]. In context of the microbiome, the gLV equations have been used to model the population dynamics of gut microbial communities [15], and are given by

$$\frac{d}{dt}y_i(t) = y_i(t)\left(\rho_i + \sum_{j=1}^N K_{ij}y_j(t)\right), \quad (1)$$

where $y_i(t)$ denotes the abundance of microbes of species i at a given time t , ρ_i is the growth rate of species i , and K_{ij} is the interaction coefficient between two populations i and j . The interaction parameters K_{ij} form the $N \times N$ interaction matrix K , where N is the number of species. The growth rate parameters ρ_i are constrained by $\rho_i > 0$. The interaction parameters K_{ij} capture prototypical ecological interactions such as competition, symbiosis, and amensalism [15]. Specifically, the parameter K_{ij} represents the effect of species j on species i , which is mediated by environmental factors such as available nutrients. Thus, if environmental factors are changed, the parameters K_{ij} will change as well.

In general, gLV systems can exhibit periodic and chaotic behaviors [16, 17], and the criteria that predict the stability of ecosystems based on their structure have been prominently studied in theoretical ecology [18–20]. Here, we focus on ecological dynamics that relax to point attractors. In this regime, the gLV dynamics of concern can be represented by a pseudo-energy landscape (e.g. a Lyapunov function), which is a scalar field in ecological state space that behaves analogously to a physical energy landscape.

We wish to determine a coordinated modification of these interaction parameters K_{ij} that drive the system to a target state. The growth rates ρ_i and interactions K_{ij} determine the dynamical landscape on which the microbial system evolves. A modification of the interaction parameter matrix K reshapes the dynamical landscape of the gLV system. This reshaping process is visualized schematically in Fig. 1.

All simulations in this paper were run with the quadrature method `odeint` from the Python module `scipy.integrate`.

B. A gLV model fit to experimental data

In a mouse experiment, Buffie *et al.* demonstrated that mice that are administered the antibiotic clindamycin become susceptible to *Clostridioides difficile* infection (CDI) [9]. Stein *et al.* fit a gLV model, referred to as the CDI model, to the time-series microbial abundance data from this mouse experiment [3]. For modeling purposes, microbial species are coarse-grained at the genus level, resulting in 11 microbial populations, each described by a population y_i in the gLV model. This gLV model captures the CDI-resistant and CDI-susceptible steady states that are observed in the experiment [3, 6].

The dynamical structure of this CDI model is characterized by the composition and stability of its steady states. Two steady states in this model, including the experimentally-observed CDI-resistant state, are locally stable (i.e., the eigenvalues of the Jacobian matrix evaluated at these steady state compositions are exclusively negative). Additionally, the CDI model features six steady states whose Jacobian matrices have one non-negative eigenvalue (referred to as having one “unstable direction”); it also features 23 steady states, including the CDI-susceptible state, whose Jacobian matrices have two non-negative eigenvalues (i.e., with two unstable directions). The CDI-susceptible state is composed of 5 coarse-grained species and the CDI-resistant state is composed of 3 coarse-grained species. In these steady states, the abundance of all other species is zero. The detailed compositions of these steady states are given in the Supplementary Information.

In this paper, we examine the transition between the CDI-susceptible state and the CDI-resistant state, and apply SPARC to the bistable region formed by these states. First, we demonstrate SPARC in the “infection” scenario in which the CDI-susceptible steady state is treated as the target state and the CDI-resistant steady state is designated the alternative state. We consider an initial condition on the plane spanned by the target state \vec{y}_a and the alternative state \vec{y}_b that tends towards \vec{y}_b in the absence of any intervention. The goal of SPARC is to find a modification to the interaction matrix ΔK that alters the evolution of this initial condition and drives it towards the target state. In the infection scenario, this parameter change represents a disruption of the micro-

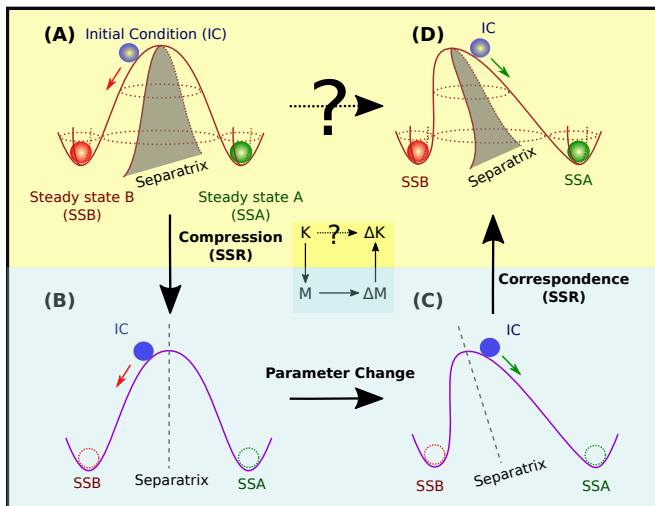


FIG. 1. **A schematic overview of how SPARC (SSR-guided parameter change) controls steady-state outcomes.** (A) A bistable region in a high-dimensional gLV model, with two steady states and an initial condition tending towards the alternative steady state (shown in red), is represented as a pseudo-energy (Lyapunov) landscape. This landscape is parameterized by the interaction matrix K of the high-dimensional gLV system. (B) The high-dimensional landscape is compressed into a reduced 2-dimensional landscape, generated by the dimensionality-reduction technique steady-state reduction (SSR) as described in Eq. (4). This 2D landscape is parameterized by a 2×2 interaction matrix M . (C) Guided by a bifurcation analysis of this reduced 2D system, a modification of the interaction matrix ΔM changes the Lyapunov landscape in a targeted way. After this change, the initial condition tends towards the healthy steady state (shown in green) in the low-dimensional system. (D) A high-dimensional parameter modification ΔK , informed by the 2D parameter change ΔM via the SSR formulae, changes the high-dimensional Lyapunov landscape. It is computationally difficult to identify this parameter change directly from the original model (A to D), but using SSR and the bifurcation analysis of the 2D model, this change is straightforward (A to B to C to D).

bial dynamics that can drive the system towards a state susceptible to CDI.

We later consider the “recovery” scenario in which the target state is the CDI-resistant state and the alternative state is the CDI-susceptible state. In this scenario too, SPARC alters the steady-state behavior of an initial condition so that it flows towards the target CDI-resistant state. The parameter change generated by SPARC in this scenario informs the intervention needed to recover from the CDI-susceptible state in this model. These results demonstrate that, for this pair of

steady states in the CDI model, SPARC is able to drive microbial dynamics in the direction of either steady state.

C. SSR-guided parameter change (SPARC)

We develop a multi-step control framework to determine a parameter change that drives a given initial condition towards a target state. A bistable landscape of interest in a high-dimensional gLV model is first reduced into a 2D gLV model using steady-state reduction (SSR) [11]. This control framework is called SPARC (SSR-guided parameter change), and summarized in Fig. 1.

1. Steady-state reduction

Steady-state reduction (SSR), developed by Jones and Carlson, is a mathematical technique that compresses a high-dimensional gLV system into a 2D gLV system, as shown in Fig. 1A and B [11]. In a high-dimensional gLV model of N species, there are N^2 interaction parameters. Due to the complexity of the feedbacks of the ecological system, it is analytically intractable and computationally expensive to numerically determine how modifications of interaction parameters affect the asymptotic behavior of arbitrary initial conditions.

To understand the dynamics in the high-dimensional phase space, we consider bistable systems and focus on the subspace spanned by the two steady states \vec{y}_a and \vec{y}_b . The SSR technique views steady states \vec{y}_a and \vec{y}_b of the high-dimensional model as idealized composite states and constructs a new set of 2D gLV equations in which the basis vectors correspond to the high-dimensional steady states. This 2D gLV system approximates the slow manifold that connects \vec{y}_a and \vec{y}_b , and is the best possible gLV approximation of the high-dimensional dynamics on the subspace spanned by \vec{y}_a and \vec{y}_b [11]. Explicitly, the approximate 2D gLV system has the form

$$\begin{aligned} \frac{dx_a}{dt} &= x_a(\mu_a + M_{aa}x_a + M_{ab}x_b), \text{ and} \\ \frac{dx_b}{dt} &= x_b(\mu_b + M_{ba}x_a + M_{bb}x_b), \end{aligned} \quad (2)$$

where x_a corresponds to the high-dimensional gLV system’s component in the direction $\hat{x}_a = \frac{\vec{y}_a}{\|\vec{y}_a\|_2}$, x_b corresponds to the direction $\hat{x}_b = \frac{\vec{y}_b}{\|\vec{y}_b\|_2}$, and $\|\vec{v}\|_2$ is the 2-norm of \vec{v} . The parameters μ_a and μ_b represent the growth rates of x_a and x_b , and the M_{ij} interaction parameters form a 2D interaction matrix M . SSR yields the reduced interspecies interaction parameters M_{ab} and M_{ba} , which are given by

$$\begin{aligned}
M_{ab} &= \frac{\sum_{i,j=1}^N K_{ij}(y_{ai}y_{bj} + y_{bi}y_{aj}) \left(y_{ai} - y_{bi} \sum_{k=1}^N y_{ak}y_{bk} \right)}{1 - \left(\sum_{i=1}^N y_{ai}y_{bi} \right)^2}, \text{ and} \\
M_{ba} &= \frac{\sum_{i,j=1}^N K_{ij}(y_{bi}y_{aj} + y_{ai}y_{bj}) \left(y_{bi} - y_{ai} \sum_{k=1}^N y_{bk}y_{ak} \right)}{1 - \left(\sum_{i=1}^N y_{bi}y_{ai} \right)^2},
\end{aligned} \tag{3}$$

where y_{ai} and y_{bi} are the i th components of the unit vectors $\hat{y}_a \equiv \vec{y}_a / \|\vec{y}_a\|_2$ and $\hat{y}_b \equiv \vec{y}_b / \|\vec{y}_b\|_2$, respectively. The other 2D parameters μ_a , μ_b , M_{aa} , and M_{ab} are given by

$$\begin{aligned}
\mu_\gamma &= \frac{\bar{p} \cdot \vec{y}_\gamma^{\circ 2}}{\|\vec{y}_\gamma\|_2^2}, \text{ and} \\
M_{\gamma\delta} &= \frac{(\vec{y}_\gamma^{\circ 2})^T K \vec{y}_\delta}{\|\vec{y}_\gamma\|_2^2 \|\vec{y}_\delta\|_2},
\end{aligned} \tag{4}$$

where $\gamma, \delta \in a, b$. When the high-dimensional steady states \vec{y}_a and \vec{y}_b are orthogonal, the interspecies interaction parameters M_{ab} and M_{ba} in Eq. (3) reduce to the interaction parameters in Eq. (4). In these formulae, $\vec{y}^{\circ 2} \equiv \text{diag}(\vec{y})\vec{y}$ is the element-wise square of \vec{y} . Note that SSR maps the high-dimensional steady states \vec{y}_a and \vec{y}_b to the points $(\|\vec{y}_a\|_2, 0)$ and $(0, \|\vec{y}_b\|_2)$, which are the steady states of the 2D model. Additionally, if the high-dimensional steady states are stable, SSR guarantees that their low-dimensional counterparts are stable as well. The fidelity of the SSR method is demonstrated in Fig. 3, where it is applied to an experimentally-derived gLV system. Additional examples are provided in the Supplementary Information.

2. Bifurcation analysis

After the high-dimensional gLV model is reduced to a 2D model, the next step is to find a parameter change in the 2D model that changes the steady-state behavior of the system, as shown in Fig. 1B and C. Simplifying the high-dimensional system using SSR results in a 2D gLV model with two growth rate parameters, μ_a and μ_b and four interaction parameters, M_{aa} , M_{ab} , M_{ba} , and M_{bb} .

When the steady states of the original high-dimensional bistable system are stable, SSR guarantees two stable steady states at $(1, 0)$ and $(0, 1)$. In addition to these two steady states, the system possesses a trivial unstable steady state at $(0, 0)$, and another hyperbolic fixed point with nonzero x_a and x_b components. The separatrix, which delineates the basins of attraction of the $(1, 0)$ and $(0, 1)$ steady states, is topologically required to pass through this hyperbolic fixed point.

When nondimensionalized, the 2D gLV equations

Eq. (2) become

$$\begin{aligned}
\frac{d\tilde{x}_a}{dT} &= \tilde{x}_a(1 - \tilde{x}_a - \tilde{M}_{ab}\tilde{x}_b), \text{ and} \\
\frac{d\tilde{x}_b}{dT} &= \tilde{x}_b(\tilde{\mu}_b - \tilde{M}_{ba}\tilde{x}_a - \tilde{x}_b),
\end{aligned} \tag{5}$$

where $\tilde{x}_a = -\frac{M_{aa}}{\mu_a}x_a$, $\tilde{x}_b = -\frac{M_{bb}}{\mu_b}x_b$, $T = \mu_a t$, $\tilde{M}_{ab} = M_{ab}/M_{bb}$, $\tilde{M}_{ba} = M_{ba}/M_{aa}$, and $\tilde{\mu}_b = \mu_b/\mu_a$. In terms of these nondimensionalized parameters, the two steady states are now at $(1, 0)$ and $(0, \tilde{\mu}_b)$. The coordinate of the hyperbolic fixed point is given by

$$\left(\frac{\tilde{M}_{ab}\tilde{\mu}_b - 1}{\tilde{M}_{ab}\tilde{M}_{ba} - 1}, \frac{\tilde{M}_{ba} - \tilde{\mu}_b}{\tilde{M}_{ab}\tilde{M}_{ba} - 1} \right). \tag{6}$$

Since the separatrix passes through this steady state, adjusting the parameters \tilde{M}_{ab} and \tilde{M}_{ba} alters its position and stability, as shown in Fig. 2.

A necessary condition for the steady states $(1, 0)$ and $(0, \tilde{\mu}_b)$ to be stable is that $\tilde{M}_{ab}\tilde{M}_{ba} - 1 > 0$ [11]. Thus, when \tilde{M}_{ab} is made smaller than $1/\tilde{\mu}_b$ with \tilde{M}_{ba} fixed, the \tilde{x}_a coordinate of the unstable steady state becomes negative. Equivalently, in Fig. 2 this corresponds to system moving from the top-right configuration to the top-left configuration. A linearized stability analysis finds that the topological structure of the 2D phase space also changes after this parameter change is made. As shown in the top-left panel of Fig. 2, the steady state at $(0, \tilde{\mu}_b)$ becomes unstable once \tilde{M}_{ab} is smaller than $1/\tilde{\mu}_b$, which forces initial conditions in the top-right quadrant of the phase space towards the stable state at $(1, 0)$. Similarly, once \tilde{M}_{ba} is smaller than $\tilde{\mu}_b$, the \tilde{x}_b coordinate of the hyperbolic steady state becomes negative. In Fig. 2 this corresponds to crossing from the top-right to the bottom-right, at which point the steady state at $(1, 0)$ becomes unstable. The bifurcation diagram in Fig. 2 provides a guide for how the steady-state structure of the 2D gLV equations depends on the interaction parameters.

This bifurcation analysis indicates how to move the separatrix in a particular direction. Numerical methods determine the minimal change of parameters \tilde{M}_{ab} or \tilde{M}_{ba} that switch the asymptotic steady-state behavior of a given initial condition. In simulations where the target steady state is located at $(1, 0)$, the value of \tilde{M}_{ab} is decreased incrementally, spanning from its original value

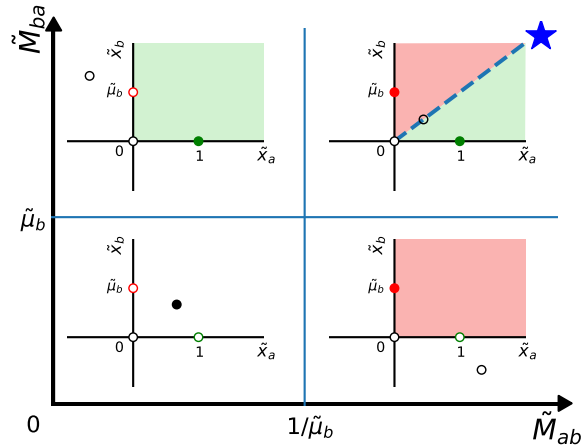


FIG. 2. **A bifurcation diagram of nondimensionalized 2D gLV systems.** This diagram shows phase space representations of different topological classes of 2D gLV dynamical landscapes, and their dependence on the nondimensionalized parameter values \tilde{M}_{ab} , \tilde{M}_{ba} , and $\tilde{\mu}_b$ of Eq. (5). The lines at $\tilde{M}_{ab} = 1/\tilde{\mu}_b$ and $\tilde{M}_{ba} = \tilde{\mu}_b$ split the parameter space into four quadrants that each correspond to a different topological configuration of phase space. The graph inside each quadrant shows a representative phase space configuration of the nondimensionalized gLV system, where \tilde{x}_a and \tilde{x}_b are the rescaled populations in Eq. (5). The hollow dots represent unstable steady states, and the filled dots represent stable steady states. The basins of attraction of the steady states $(1, 0)$ and $(0, \tilde{\mu}_b)$ are shaded in green and red, respectively. The upper-right quadrant, labeled with a blue star, represents the parameter regime in which bistable 2D landscapes occur. An alternative visualization of this bistable landscape is schematized in Fig. 1 as a pseudo-energy landscape. The reduced 2D gLV models, generated by applying SSR to bistable regions in high-dimensional gLV models, reside in this upper-right quadrant. In this bistable quadrant, the separatrix passes through the hyperbolic steady state with non-negative coordinates. The steady states at $(1, 0)$ and $(0, \tilde{\mu}_b)$ undergo transcritical bifurcations in response to changes in \tilde{M}_{ab} and \tilde{M}_{ba} , yielding the diagrams in adjacent panels. The lower-left quadrant is included for completeness.

through $1/\tilde{\mu}_b$. In terms of the dimensionalized 2D gLV system, this corresponds to keeping M_{bb} constant while M_{ab} is modified until the separatrix is shifted to a position where the initial condition switches from one basin of attraction to the other.

3. Correspondence between 2D and high-dimensional gLV models

Changes in the 2D interaction parameters that drive an initial condition to a target state are associated with changes in the high-dimensional interaction parameters, since the 2D reduced parameters are functions of the high-dimensional parameters via the SSR formulae. This

is schematically shown in the transition from Fig. 1C to Fig. 1D. More explicitly, Eq. (4) can be re-written as

$$M_{\gamma\delta} = \sum_{i,j} \alpha_{ij}^{\gamma\delta} (\bar{y}_a, \bar{y}_b) K_{ij}, \quad (7)$$

where $\gamma, \delta \in \{a, b\}$, and \bar{y}_a and \bar{y}_b are the two steady states of interest. In this paper, since the target state is placed at $(1, 0)$, it is most important to modify the parameter $\tilde{M}_{ab} = M_{ab}/M_{bb}$. For simplicity we only consider modifications to M_{ab} , and therefore are primarily concerned with the coefficients α_{ij}^{ab} , hereafter referred to as α_{ij} . Thus, from this correspondence a modification in the 2D interaction matrix M may be reproduced in the high-dimensional system by modifying the high-dimensional interaction matrix K . This choice is degenerate — there is more than one way to change the high-dimensional interaction matrix K that corresponds to the same 2D parameter modification. Note that the smallest possible high-dimensional parameter change ΔK_{ij} is associated with the largest coefficient α_{ij} .

III. RESULTS

SPARC (SSR-guided parameter change) controls the steady-state outcome of a high-dimensional gLV system by deliberately changing the geometry of its dynamical landscape. SPARC (i) approximates a bistable landscape of a high-dimensional gLV system by its 2D SSR-generated counterpart, (ii) identifies a 2D interaction parameter change that switches the asymptotic behavior of an initial condition on this bistable landscape, and (iii) associates the 2D parameter change with a parameter modification in the high-dimensional gLV system. This parameter modification shifts the high-dimensional landscape so that an otherwise disease-prone initial condition will instead tend towards the target state.

Note that since the steady states of the high-dimensional model are dependent on the interaction matrix K , a small change in this matrix will slightly modify the coordinates of the steady states. Thus, to allow the system to evolve back to the original steady states, this parameter modification must be turned off after some time. To initially demonstrate SPARC, the parameter modification is turned off once the system stabilizes at the shifted steady state (Fig. 3). When SPARC is applied to the CDI model, the parameter modification is small enough that the changes in steady state locations are negligible (Supplementary Information). Later, when considering the “recovery” scenario, the parameter modification is turned off before the system stabilizes at any steady state; in this case there is a critical duration that the parameter modification must be active for in order for the intervention to be successful (Fig. 5).

In this section, SPARC is first applied to the CDI model fit by Stein *et al.* to data from a *Clostridioides difficile* infection (CDI) experiment in mice [3]. Then,

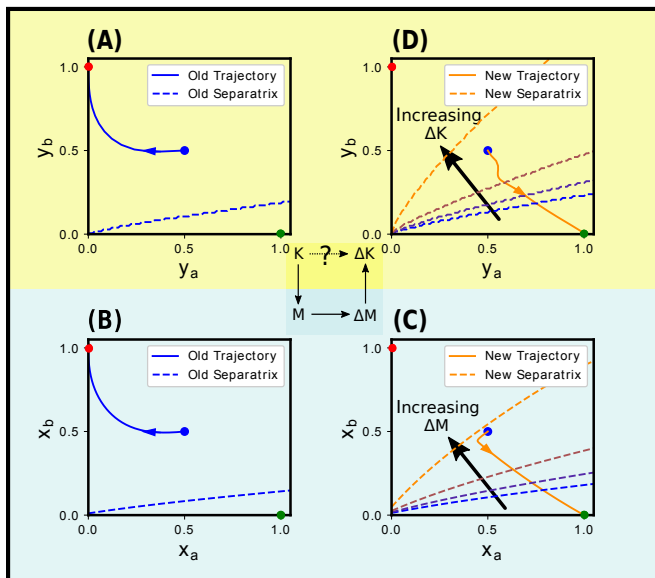


FIG. 3. **A realization of SPARC, as described in Fig. 1, applied to the infection scenario of the CDI model.** (A) The phase space of the CDI model [3] is projected onto the 2D plane spanned by the target steady state \vec{y}_a and the alternative steady state \vec{y}_b . The target and alternative steady states at $(\|\vec{y}_a\|_2, 0)$ and $(0, \|\vec{y}_b\|_2)$ are rescaled in this plot to the points $(1, 0)$ and $(0, 1)$. The in-plane separatrix, generated numerically, delineates the basins of attraction. (B) Steady-state reduction (SSR) generates an approximate 2D phase space. Notice that the 2D separatrix and trajectory qualitatively resemble those in (A). (C) The 2D separatrix moves as the 2D interaction matrix M is modified. Four separatrices corresponding to four changes with increasing magnitude in the interaction matrix ΔM are shown. The matrix element and direction of this change are guided by the bifurcation analysis in Fig. 2. A sufficiently large parameter change alters the steady-state outcome of the initial condition $(0.5, 0.5)$. (D) Changes in the low-dimensional interaction parameter ΔM are associated with changes in high-dimensional parameter ΔK by SSR formulae. The resulting shift in the high-dimensional separatrix is qualitatively similar to that of the low-dimensional system. In particular, the initial condition $(0.5\vec{y}_a + 0.5\vec{y}_b)$ now evolves towards the target steady state. SPARC successfully alters the steady-state outcome without having to search a 121-dimensional parameter space.

the robustness of SPARC is examined by applying it to synthetic gLV models.

A. Steady-state reduction (SSR) produces a 2D approximation to bistable dynamics in a high-dimensional gut microbiome model

First, bistable dynamics in the CDI model are approximated by reduced dynamics on a 2D subspace generated by steady-state reduction (SSR). We focus on two steady states of this gLV model that correspond to experimentally observed CDI-resistant and CDI-susceptible microbiome compositions. For the initial demonstration of SPARC, we consider the “infection” scenario in which

the CDI-susceptible state is defined as the target state and the CDI-resistant state is defined as the alternative state.

The target state and the alternative state are represented by the high-dimensional vectors \vec{y}_a and \vec{y}_b , respectively. The microbial dynamics that result from the initial condition $(0.5\vec{y}_a + 0.5\vec{y}_b)$ tend towards the alternative steady state \vec{y}_b . To visualize these dynamics, the trajectory is projected onto a plane spanned by the steady states \vec{y}_a and \vec{y}_b , as displayed in Fig. 3A. In this figure, the axes are rescaled so that the steady state \vec{y}_a is located at point $(1, 0)$ and the steady state \vec{y}_b is located at point $(0, 1)$. The separatrix shown in Fig. 3A is numerically generated from trajectory simulations. Notice that on this subspace, the initial condition is above the separatrix, and hence the initial condition evolves towards the alternative steady state at $(0, 1)$.

This 11D bistable landscape is approximated by a reduced 2D gLV model generated by SSR, according to Eq. (4). The SSR-generated parameter values and their nondimensionalized counterparts are provided in the Supplementary Information. The dynamics of the reduced 2D trajectory were initial condition $(0.5, 0.5)$ are displayed in Fig. 3B, and are similar to the projection of the 11D dynamics in Fig. 3A. Note that the position of the separatrix, which is generated analytically in the 2D model [11], is well-approximated by SSR. In the Supplementary Information it is further demonstrated that this reduced 2D model accurately approximates the high-dimensional trajectories that originate from other initial conditions.

It is difficult to identify the interspecies feedbacks that induce bistability in a high-dimensional system: in general, it is unclear how the separatrix changes as a function of the system parameters. On the other hand, in the reduced 2D gLV system, there are well-defined conditions for bistability, namely

$$\begin{aligned} \tilde{M}_{ab}\tilde{\mu}_b &= (M_{ab}/M_{bb})(\mu_b/\mu_a) > 1, \quad \text{and} \\ \tilde{M}_{ba} &= M_{ba}/M_{aa} > \tilde{\mu}_b = \mu_b/\mu_a. \end{aligned} \quad (8)$$

Since these low-dimensional parameters M_{ab} and M_{ba} are linear combinations of the high-dimensional parameters K_{ij} , the conditions for bistability can be decomposed into their relative contributions from the high-dimensional interspecies feedbacks K_{ij} .

Specifically, consider the numerators of these inequalities, $M_{ab} = \sum_{ij} \alpha_{ij}^{ab} K_{ij}$ and $M_{ba} = \sum_{ij} \alpha_{ij}^{ba} K_{ij}$ (as in Eq. (7)). Then, the relative contributions to M_{ab} by each of the $\alpha_{ij}^{ab} K_{ij}$ terms may be compared (and likewise for M_{ba}). When \vec{y}_a corresponds to the CDI-susceptible state and \vec{y}_b corresponds to the CDI-resistant state, the contributions to M_{ab} are dominated by the inhibition of *Barnesiella* on both *Blautia* and undefined genus of *Enterobacteriaceae* (i.e., the contributions $\alpha_{9,1}^{ab} K_{9,1}$ and $\alpha_{5,1}^{ab} K_{5,1}$). Contributions to M_{ba} are dominated by the inhibition of undefined genus of *Enterobacteriaceae* and *Blautia* on unclassified *Lachnospiraceae* and *Barnesiella*

(i.e., the contributions $\alpha_{3,9}^{ba}K_{3,9}$, $\alpha_{3,5}^{ba}K_{3,5}$, $\alpha_{1,9}^{ba}K_{1,9}$, and $\alpha_{1,5}^{ba}K_{1,5}$). Additional details about these contributions are provided in the Supplementary Information. Thus, the bistability between steady states \vec{y}_a and \vec{y}_b is largely driven by feedbacks between a pair of species present in \vec{y}_a (undefined genus of Enterobacteriaceae and Blautia) and a pair of species present in \vec{y}_b (unclassified Lachnospiraceae and Barnesiella).

B. Bifurcation analysis guides interaction parameter changes that modify steady-state outcomes in reduced 2D gLV systems

Next, the bifurcation analysis of 2D gLV systems depicted in Fig. 2 indicates how to drive an initial condition $(0.5, 0.5)$ towards the target steady state $(1, 0)$. This requires enlarging the basin of attraction of the steady state $(1, 0)$, which is equivalent to rotating the separatrix counter-clockwise. The SSR-generated 2D system is bistable, and thus belongs to the topological class in the upper-right quadrant of Fig. 2. Accordingly, the parameter M_{ab} is decreased. When $M_{ab} = M_{bb}\mu_a/\mu_b$, the alternative steady state at $(0, 1)$ becomes unstable, guaranteeing the initial condition $(0.5, 0.5)$ will tend towards the target state at $(1, 0)$. However, to identify the minimal intervention that drives the system towards the target state, we consider intermediate steps between the original value of M_{ab} and the bifurcation point $M_{bb}\mu_a/\mu_b$.

Four incremental parameter changes are plotted in Fig. 3C. On the fourth step, the separatrix is sufficiently modified so that the initial condition tends towards the target healthy steady state. The original 2D interaction matrix M , the parameter change to M_{ab} , and the resulting interaction matrix $M + \Delta M$ are visualized in Fig. 4E-G. The trajectory plots in the bottom-left and the bottom-right corners of Fig. 4 illustrate the behavior of the 2D gLV system parameterized by M and $M + \Delta M$, respectively. Therefore, SPARC can identify and modify interaction parameters to switch the steady state behavior of this 2D model.

C. SSR maps low-dimensional bifurcation behavior to the high-dimensional system

Finally, having determined the low-dimensional parameter modification that alters the separatrix in the reduced 2D model (as shown in Fig. 3C), corresponding high-dimensional parameters that alter the system outcome in the original model can be identified. Due to the degeneracy associated with mapping from the low-dimensional to high-dimensional parameters, as is clear in the SSR formulae given by Eq. (4), there are numerous modifications to the high-dimensional interaction matrix K that correspond to the same change in the 2D interaction matrix, as shown in Fig. 4D. In the CDI model, if the parameter change is confined to only one element of

K , there are a total of 121 choices. In order to make the smallest change in the interaction matrix K , the coefficient K_{ij} corresponding to the largest α_{ij} value is chosen, as described in Eq. (7). Specifically, the parameter change $\Delta K_{5,3} = 0.1744$ is used.

In Fig. 4D the magnitudes of the α_{ij} coefficients are plotted, and the largest coefficient is highlighted with a dashed box. In the bottom row of Fig. 4, the original K matrix (panel A), the required modification ΔK corresponding to that α_{ij} coefficient (panel B), and the resulting modified interaction matrix $K + \Delta K$ (panel C) are displayed. The trajectories in the upper-left and upper-right corners indicate the behavior of the systems parameterized by K and $K + \Delta K$, respectively.

Fig. 3D displays the results of a representative 11D interaction matrix change ΔK that drives the initial condition to the target state \vec{y}_a . As in Fig. 3C, four incremental parameter changes that each modify the separatrix are plotted. The largest of these four parameter changes rotates the 11D separatrix counter-clockwise so that the initial condition $(0.5\vec{y}_a + 0.5\vec{y}_b)$ tends towards the healthy steady state \vec{y}_a . Although small discrepancies exist between Fig. 3C and Fig. 3D due to the SSR approximation, SPARC successfully alters the steady-state outcome of a high-dimensional gLV system by deliberately changing its interaction parameters.

D. SPARC generates a finite-time intervention that drives a disease-prone initial condition towards a healthy state in the CDI model

Next, we consider the recovery scenario in which the “healthy” CDI-resistant state is the target state \vec{y}_a and the “diseased” CDI-susceptible state is the alternative state \vec{y}_b . The initial condition at $(0.1\vec{y}_a + 0.9\vec{y}_b)$ is chosen to demonstrate that SPARC can be effective even when the initial condition is closer to the alternative state than to the target state. As in the previous case, SPARC is applied to change the steady-state outcome of this initial condition, which is shown in Fig. 5. For clarity, the shifted separatrices in Fig. 5C and D are not displayed.

Without any parameter modification, the bistable region is exactly the reflection of the previous case, as shown in Fig. 5A and B. However, the parameter modification generated by SPARC shifts the separatrix in the opposite direction. In this case, the separatrix is already close to the alternative steady state at $(0, 1)$. The 2D parameter modification makes $\tilde{M}_{ab} < 1/\tilde{\mu}_b$, resulting in the steady state at $(0, 1)$ becoming unstable, as shown in Fig. 2 (top-right and top-left panels). Therefore, although the initial condition is nearby the alternative steady state, after modifying the low-dimensional parameters it tends towards the target state at $(1, 0)$.

The successful 2D parameter change is projected to the high-dimensional model. Notably, the applied parameter change causes the steady state \vec{y}_b in the high-dimensional model to become unstable. Thus SPARC is capable of al-

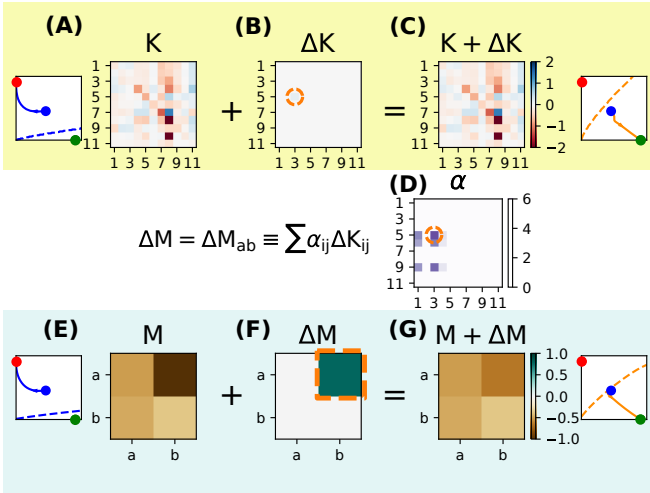


FIG. 4. Realization of the SSR-guided changes to gLV interaction parameters. As described in SPARC, the original high-dimensional interaction matrix K (A), SSR-guided parameter change ΔK (B), and the resulting interaction matrix $K + \Delta K$ (C) are displayed. The steady-state reduced parameter matrix M (E), bifurcation analysis guided parameter change ΔM (F), and the resulting 2D interaction matrix $M + \Delta M$ (G) are also displayed. The low-dimensional parameter change ΔM , is related to high-dimensional parameter changes through the SSR formulae Eq. (4). The α_{ij} coefficients represent the weights of the elements of the high-dimensional interaction matrix K in the steady-state reduced interaction matrix M , as in Eq. (7) and these coefficients are visualized in panel (D). To minimize the size of the high-dimensional parameter change, the interaction parameter K_{ij} that corresponds to largest coefficients α_{ij} is chosen to be modified. In this case, the coefficient $\alpha_{5,3}$ is the largest, which determines the choice of ΔK . The phase space diagrams in each corner illustrate the trajectory of the initial condition $(0.5\vec{y}_a + 0.5\vec{y}_b)$ or $(0.5, 0.5)$, for each of the adjacent interaction matrices.

tering the stability properties of high-dimensional steady states, which enables the control of initial conditions even when they are located at or nearby an alternative steady state.

Fig. 5D also shows the effect of the duration of the parameter modification. For SPARC to succeed, the parameter modification needs to be active long enough for the microbial state to escape its original basin of attraction. The red trajectory in Fig. 5 demonstrates that the system returns back to the alternative steady state if the parameter change is applied for too short of a duration. The green trajectory illustrates that the system will evolve towards the target state as long as the parameter change is active beyond a critical duration. This critical duration varies from case to case and was determined here numerically by trial-and-error. The orange trajectory occurs when the parameter change is active until the system stabilizes at the shifted steady state, as in Fig. 3.

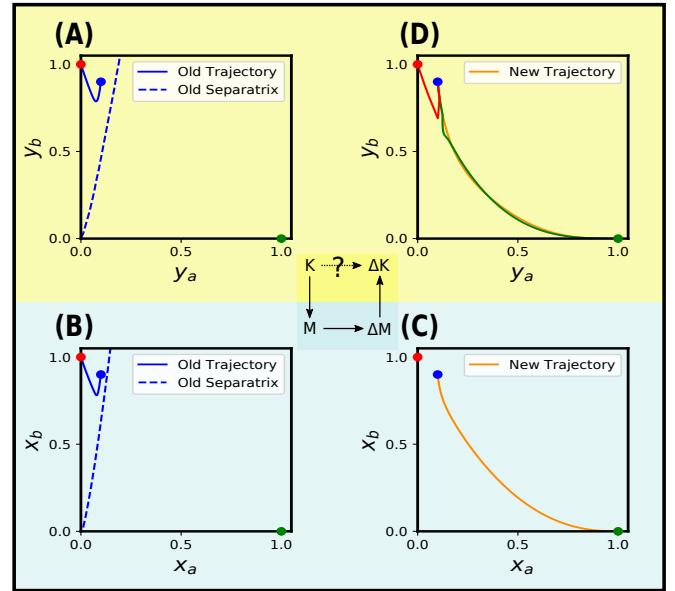


FIG. 5. A realization of SPARC applied to the CDI model in the recovery scenario. Here, the target state \vec{y}_a is the CDI-resistant state and the alternative state \vec{y}_b is the CDI-susceptible state. The target and alternative steady states at $(\|\vec{y}_a\|_2, 0)$ and $(0, \|\vec{y}_b\|_2)$ are rescaled in this plot to the points $(1, 0)$ and $(0, 1)$. (A) With the positions of the steady states switched, the 2D projection of the high-dimensional bistable region shown in Fig. 3 is redrawn. Here the separatrix is close to the alternative state \vec{y}_b . The initial condition at $0.1\vec{y}_a + 0.9\vec{y}_b$ tends towards the alternative state \vec{y}_b . (B) The SSR formulae are applied to generate a 2D approximate model. (C) After a parameter change ΔM_{ab} , the steady state at $(0, 1)$ becomes unstable and the initial condition now tends towards the target state. (D) The parameter change in the 2D model is associated with a parameter change in the original CDI model. The yellow line plots the trajectory when the parameter modification is turned off after the system stabilizes, as in the case of Fig. 3. The red line shows the trajectory when the parameter change is turned off before the critical time, and the green line shows the trajectory when the parameter change is turned off after the critical time.

E. SPARC successfully changes steady state outcomes in synthetic gLV models

1. “Permuted” synthetic models

To verify that SPARC is generalizable, it is applied to 100 synthetic parameter sets generated by permuting the interaction parameters of the CDI model. In these synthetic parameter sets, the growth rates ρ_i are kept the same as in the CDI model. The diagonal entries of the interaction matrix K are all negative (as shown in Fig. 4A), which is biologically reasonable since positive diagonal entries imply unphysical infinite growth. To ensure the synthetic data sets preserve this property, the diagonal and off-diagonal entries of the K matrix are permuted independently. All 100 parameter sets are generated in this way. This permutation process is demonstrated in

Fig. 6A and B.

In the next step, bistable regions for each synthetic system must be identified in order for SPARC to be applicable. Steady state analysis shows that, for a randomly permuted parameter set, stable steady states are small in number. From 100 permuted gLV parameter sets, there are on average 0.8 completely stable steady states and 5.3 steady states with at most one unstable direction (i.e., steady states whose Jacobian matrices have at most one non-negative eigenvalue) per parameter set.

To ensure there are enough steady states to form bistable landscapes, we compute all 2^N steady states of each synthetic parameter set, then identify all steady states whose Jacobian has 0 or 1 positive eigenvalues in each parameter set, and use numerical simulations to test whether each steady state pair forms a bistable landscape. Specifically, for a steady state pair \vec{y}_a and \vec{y}_b , trajectories with initial conditions $(0.95\vec{y}_a + 0.05\vec{y}_b)$ and $(0.05\vec{y}_a + 0.95\vec{y}_b)$ are simulated to test whether they tend towards their nearest steady state. In addition, if initial conditions at $(0.8\vec{y}_a + 0.2\vec{y}_b)$ or $(0.2\vec{y}_a + 0.8\vec{y}_b)$ tend towards some other third steady state, the steady state pair is excluded. Out of the 100 synthetic parameter sets, a total of 136 bistable landscapes were identified.

In this context, SPARC is considered successful if it identifies high-dimensional interaction parameter changes that alter the steady-state outcome in a bistable system, as in Fig. 6C. This success relies on the correspondence between the 11D and 2D landscapes generated by SSR, the bifurcation analysis of the 2D system, and the correspondence between 2D and 11D parameters governed by the SSR formulae. Therefore, if an initial condition in both the unperturbed 11D and 2D models tends towards the same steady state, and the same initial condition in both the perturbed 11D and 2D models tend towards the other steady state in the bistable landscape, SPARC is considered successful.

To examine the fidelity of SPARC on synthetic parameter sets, it is applied to an ensemble of synthetically generated models. The two steady states of the synthetic bistable system are arbitrarily labeled as \vec{y}_a and \vec{y}_b . In Fig. 3 the initial condition was located at $(0.5\vec{y}_a + 0.5\vec{y}_b)$, but for these synthetic parameter sets the initial condition is located at $(0.2\vec{y}_a + 0.8\vec{y}_b)$. Since SSR is more accurate near the two steady states, this choice of initial condition improves the success rate of SPARC. SPARC can fail at two steps, corresponding to the arrows A to B and C to D in the schematic Fig. 1. The first type of error occurs when SSR fails to preserve the steady state behavior of the gLV model; this error is demonstrated in Fig. 6D, where the high-dimensional initial condition tends towards steady state \vec{y}_b but the initial condition of the SSR-reduced model tends towards steady state \vec{x}_a . The second type of error occurs when associating the low-dimensional parameter change with a high-dimensional parameter change; this error is demonstrated in Fig. 6E, where the modified low-dimensional trajectory correctly tends towards steady state \vec{x}_a , but its corresponding

high-dimensional trajectory erroneously tends towards steady state \vec{y}_b . Since the choice of a high-dimensional parameter change is degenerate, modifications to four interaction parameters K_{ij} corresponding to the four largest α_{ij} coefficients are tested. Small changes in the interaction matrix K will slightly change the location of the steady states, so this perturbation is turned off after the system has relaxed to the shifted steady states to allow the system to return to its original steady states.

Out of the 136 bistable landscapes generated from 100 synthetic parameter sets, SPARC successfully identified parameter modifications that led to the targeted transition between steady-state outcomes 57% (77/136) of the time. Details about specific error rates occurred are provided in Fig. 6F: 17% (23/136) occurred during the SSR compression step, and 26% (36/136) occurred during the mapping from the 2D parameters to high-dimensional parameters. Manual intervention (e.g., trying different sizes of the prescribed parameter change) can improve this success rate. Therefore, SPARC is effective at altering steady-state behavior in generic gLV systems.

2. “Noisy” synthetic models

Finally, since inferring parameter values in gLV systems is an intrinsically noisy procedure, it is valuable to understand whether parameter changes generated by SPARC are robust to noise in the fitted parameters. We consider the “infection” scenario in which the CDI-susceptible state is the target state \vec{y}_a and the CDI-resistant state is the alternative state \vec{y}_b . Implementing the parameter change prescribed by SPARC ($\Delta K_{5,3} = 0.1744$) successfully drives an initial condition at $(0.5\vec{y}_a + 0.5\vec{y}_b)$ towards the target state \vec{y}_a . To test the robustness of the SPARC method, this parameter change is applied to synthetic “noisy” systems that are generated by independently scaling each interaction parameter K_{ij} by a number randomly drawn from a uniform distribution between $1 - \beta$ and $1 + \beta$. This parameter β is called the “noise.” In the Supplementary Information the following analysis is also performed using a parameter change 20% larger than the original one ($\Delta K_{5,3} = 0.2092$). This increment compensates for the deviation between the original and the SSR-generated separatrices.

The steady states of these synthetic systems are functions of the interaction parameters, and therefore differ from the steady states of the original CDI model. In gLV systems the presence/absence combination of species uniquely identifies a steady state, so it is straightforward to identify the two steady states in these noisy systems, called $\tilde{\vec{y}}_a$ and $\tilde{\vec{y}}_b$, that correspond to the target and alternative steady states \vec{y}_a and \vec{y}_b of the original CDI model. Many of these newly-generated steady states are biologically unreasonable: for a noise of $\beta = 0.025$, nearly half of the noisy steady states $\tilde{\vec{y}}_a$ contain negative entries. Additional details regarding the deviations of the noisy steady states as a function of the noise β are provided in

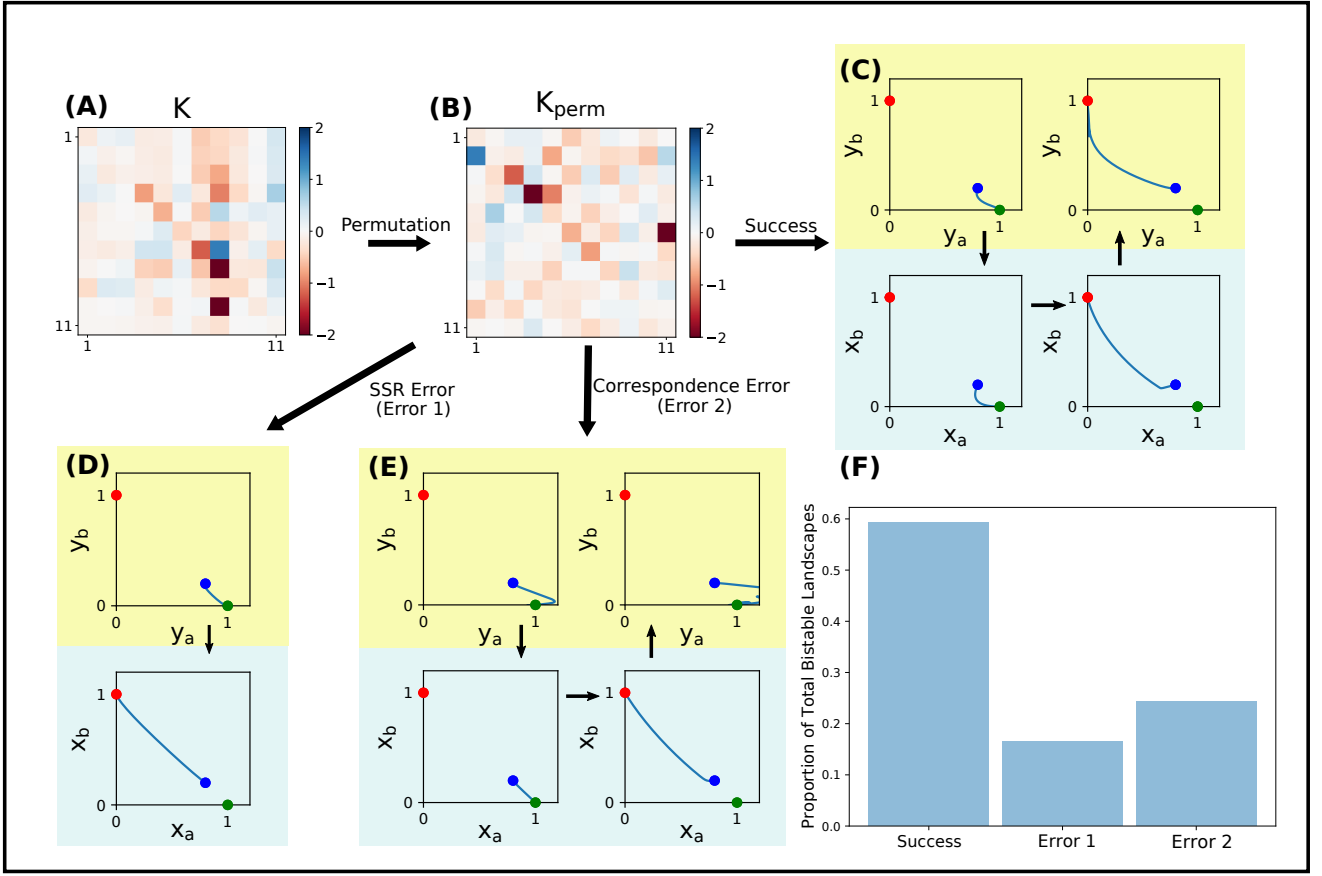


FIG. 6. **SPARC is effective at modifying steady-state outcomes in synthetic gLV models.** (A, B) The interaction matrix K from the CDI model is randomly permuted to generate 100 synthetic parameter sets. From these 100 synthetic gLV systems, 140 bistable regions are identified. SPARC is applied to these synthetic models. (C) SPARC is considered successful if the parameter modification changes the trajectory of the initial condition so that it tends towards the target state (green), rather than the alternative state (red). (D, E) Two types of errors in SPARC are possible. SPARC can fail during the steady-state reduction process if the outcome of the high-dimensional system does not agree with the steady-state outcome of the reduced system (SSR Error, panel D). It can also fail if the high-dimensional parameter change ΔK does not appropriately alter the steady-state outcome (Correspondence Error, panel E). (F) SPARC successfully modifies 57% (77/136) of the synthetically-generated bistable landscapes. These numbers represent a baseline error rate of SPARC that may be further improved through manual intervention.

the Supplementary Information.

We only consider noisy synthetic systems (i) that do not contain any negative entries in the steady states \tilde{y}_a and \tilde{y}_b , and (ii) in which an initial condition at $(0.5\tilde{y}_a + 0.5\tilde{y}_b)$ flows towards the alternative state \tilde{y}_b in the absence of any intervention (note that the initial condition is based on steady states of the original CDI model). Then, the parameter change $\Delta K_{5,3} = 0.1744$ is applied to the noisy models for an initial condition $(0.5\tilde{y}_a + 0.5\tilde{y}_b)$; if the system flows towards the target state \tilde{y}_a the parameter change is considered successful, and if it does not it is considered an error. The error rate of SPARC as a function of the noise β is plotted in the Supplementary Information. For each noise value, 1000 synthetic systems are created to generate statistics for the error rates. Using the original parameter change $\Delta K_{5,3} = 0.1744$ works well for very small noise values ($\beta < 0.005$), rapidly increases to an error rate of 40%

with a noise of $\beta = 0.02$, and eventually approaches 80% for a noise of $\beta = 0.5$. With the incremented parameter change of $\Delta K_{5,3} = 0.2092$, the CDI model works nearly perfectly for synthetic systems with small noise values ($\beta < 0.02$). Then, as the noise increases the error rate worsens: a noise of $\beta = 0.1$ corresponds to a 30% error rate, and a noise of $\beta = 0.5$ approaches an 80% error rate. These analyses indicate that interventions generated by SPARC are effective for gLV systems whose parameters are known precisely, but are less effective when parameters are relatively unconstrained. Taken another way, these results place a limit on the required accuracy of parameter estimation, beyond which point two measured systems will differ enough in their parameter values that they diverge in their behavior.

IV. DISCUSSION

A. SPARC is efficient and flexible

SPARC generates a 2D gLV model to guide high-dimensional parameter modifications that alter the system outcome. Without such a guide, this parameter change must be instead selected through trial-and-error. A study about T-cell cancer networks used this exhaustive trial-and-error method to find parameter perturbations that drive the system between attractors, but it was computationally expensive to search their parameter space [21]. In gLV systems, the number of computations needed for this trial-and-error method grows as $\mathcal{O}(N^2)$, where N is the number of species in the gLV model. As the number of species N becomes large, the exhaustive method becomes computationally intractable.

Rather than exploring the N^2 -dimensional parameter space of K , SPARC allows exploration of a 2-dimensional subspace of M associated with the bistable dynamics of interest of the high-dimensional model. In the SSR-generated 2D model, parameter modifications are analytically tractable using bifurcation analysis, which determines the sign of the parameter change according to the direction of the required separatrix shift. After the 2D model parameter change is determined, SSR formulae provide a direct correspondence between the 2D and the high-dimensional parameter modifications that produce the same steady-state outcome. For example, since bistability is well-defined in the 2D gLV system, SSR reveals the interspecies feedbacks most responsible for bistability in the high-dimensional system.

Furthermore, SPARC is flexible enough to drive the dynamical system bidirectionally between steady states, as demonstrated in the infection and recovery scenarios. When one steady state in the bistable region is desirable, as in the clinically-motivated recovery scenario considered here, SPARC identifies both which parameter changes to avoid and which to perform in order to achieve the target outcome. Both types of parameter changes are informative when trying to prevent the system from tending toward an undesirable steady state.

Finally, we note that the applicability of the parameter changes recommended by SPARC is sensitive to the accuracy of the fitted gLV interaction parameters. For example, in the CDI system (as demonstrated by the noisy synthetic models), the SPARC parameter change becomes less effective as the noise in the interaction parameters increases. This analysis quantifies the tolerable level of uncertainty in fitted interaction parameters before they result in fundamentally different classes of model behavior.

B. Perturbing ecological interactions indirectly controls steady-state outcomes

Direct control methods modify the steady-state outcome of the gut microbiome by changing the state of the microbial system while retaining the same dynamical landscape. Implementations of this direct control method include bacteriotherapies such as Fecal Microbial Transplantation (FMT), which has been shown to be an effective treatment for *Clostridioides difficile* infection (CDI). FMT introduces a foreign microbial transplant that alters a host's microbiome composition, thereby ameliorating symptoms of CDI [22]. As realized in the gLV model, this amounts to an instantaneous shift in the microbial composition that moves the microbial state from one basin of attraction to another.

In contrast to this direct control method, SPARC indirectly controls the steady-state outcomes of a high-dimensional gLV model by modifying its dynamical landscape. Instead of adding foreign microbes, SPARC perturbs the interaction parameters of the gLV model, which we interpret as changing the environment in which the microbes live. Fig. 3 illustrates how this parameter-altering control method changes the steady-state outcome of a simulated gut microbial system.

SPARC could be applied to other ecological systems in order to attain a target community structure. In marine ecosystems, the target community structures may correspond to ecological states without harmful algal blooms or invasive fish species. In these cases, environmental factors such as the abundance of chemical fertilizers or pesticides, the pH, and the velocity of stream flows influence the state of the ecosystem [1, 23]. Previously, algal blooms and population dynamics of invasive fish species have been modeled with gLV systems [24, 25]. Therefore, SPARC could provide a systematic framework that guides environmental interventions to remove harmful algae or invasive fish species.

SPARC identifies a single entry in a high-dimensional interaction matrix that can be altered to change the system behavior. However, it might not be possible in practice to identify environmental factors that, when modified, change only one entry of the interaction matrix. Importantly, the parameter entry generated by SPARC is not unique, as shown in Eq. (7). As a result, it is possible to find a linear combination of changes in the environmental factors that maximize the parameter changes in the most effective entries (i.e., entries with the largest α_{ij} values) and minimize other changes, especially the most effective entries in the opposite direction. This more complex parameter change can then be simulated to assess its effectiveness.

C. SPARC provides a lens for understanding the effect of the environment on microbial composition

Having demonstrated the effectiveness of SPARC *in silico*, it would be valuable to verify this method in an experimental model system of the microbiome. SPARC relies on changing interactions between microbial species in the gut microbiome, which could be achieved by deliberately changing environmental factors in a controlled experimental setting. Therefore, any realization of this method would require an experimental microbiome model of limited microbial diversity that allows the manipulation of oxygen levels, nutrient availability, or other factors. One such experimental model might be the intestine-on-a-chip system, which simulates the human gut microbiome in a manipulable *in vitro* environment [26–28]. By fitting gLV models to time-series data from the intestine-on-a-chip, it may be possible to isolate the effect of environmental perturbations and identify the corresponding interaction matrix change ΔK underlying SPARC.

In real microbial systems, changes in environmental factors potentially affect the interactions between many species, thus changing multiple interaction parameters at a time. For example, Lin *et al.* found that four dominant bacterial genera with carbon assimilation pathways gain ecological advantages when there is a lack of dissolved carbon in the environment [29]. Therefore, environmental changes such as the removal of dissolved carbon will alter the effective microbe-microbe interactions between these species. In cases such as these, SPARC could systematically specify how environmental changes alter the dynamical landscape.

In future applications, the environmental degrees of freedom will be as myriad as diet, designer probiotics, or designer prebiotics. The combinatorial complexity of these contributions will require a systematic framework, such as SPARC, in order to understand how to drive the system towards a target state. Once environmental interventions are associated with changes in species-species

interaction parameters in gLV models, SPARC could help predict how environmental changes affect gut microbiome compositions.

V. CONCLUSION

SPARC controls the steady-state outcome of bistable regions in gLV systems by altering ecological interaction parameters. This method circumvents the computational task of performing numerical trials to exhaustively search a high-dimensional parameter space. Instead, SPARC uses a recently-developed dimensionality-reduction technique to reduce the problem to searching a 2-dimensional parameter subspace. Consequently, we are able to efficiently and systematically identify a minimal parameter change that results in desired system behavior.

SPARC provides a novel alternative to canonical control methods that modify the system state directly. SPARC instead focuses on how environmental factors and microbial interactions dictate microbial dynamics. Eventually, indirect and direct methods could be used in conjunction to provide a comprehensive framework for the control of ecological systems.

ACKNOWLEDGMENTS

This material was based upon work supported by the National Science Foundation Graduate Research Fellowship Program under Grant No. 1650114. Any opinions, findings, and conclusions or recommendations expressed in this material are those of the author(s) and do not necessarily reflect the views of the National Science Foundation. This work was also supported by the David and Lucile Packard Foundation and the Institute for Collaborative Biotechnologies through Contract No. W911NF-09-D-0001 from the U.S. Army Research Office. The funders had no role in study design, data collection and analysis, decision to publish, or preparation of the manuscript.

-
- [1] D. M. Anderson, *Ocean & Coastal Management* **52**, 342 (2009).
 - [2] R. E. Gozlan, S. St-Hilaire, S. W. Feist, P. Martin, and M. L. Kent, *Nature* **435**, 1046 (2005).
 - [3] R. R. Stein, V. Bucci, N. C. Toussaint, C. G. Buffie, G. Rtsch, E. G. Pamer, C. Sander, and J. B. Xavier, *PLOS Computational Biology* **9**, 1 (2013).
 - [4] R. E. Thresher, K. Hayes, N. J. Bax, J. Teem, T. J. Benfey, and F. Gould, *Biological Invasions* **16**, 1201 (2014).
 - [5] H. E. Jakobsson, C. Jernberg, A. F. Andersson, M. Sjlund-Karlsson, J. K. Jansson, and L. Engstrand, *PLOS ONE* **5**, 1 (2010).
 - [6] E. W. Jones and J. M. Carlson, *PLOS Computational Biology* **14**, 1 (2018).
 - [7] R. E. Thresher, *Fisheries* **33**, 114 (2008).
 - [8] P. Van den Abbeele, W. Verstraete, S. El Aidy, A. Geirnaert, and T. Van de Wiele, *Microbial Biotechnology* **6**, 335 (2013).
 - [9] C. G. Buffie, I. Jarchum, M. Equinda, L. Lipuma, A. Gobourne, A. Viale, C. Ubeda, J. Xavier, and E. G. Pamer, *Infection and Immunity* **80**, 62 (2012).
 - [10] P. J. Taylor, *Journal of Theoretical Biology* **135**, 543 (1988).
 - [11] E. W. Jones and J. M. Carlson, *Phys. Rev. E* **99**, 032403 (2019).
 - [12] O. Malcai, O. Biham, P. Richmond, and S. Solomon, *Phys. Rev. E* **66**, 031102 (2002).
 - [13] L. L. Eberhardt, *Canadian Journal of Zoology* **76**, 380 (1998).

- [14] H. Fort, *Ecological modelling* **387**, 154 (2018).
- [15] O. S. Venturelli, A. V. Carr, G. Fisher, R. H. Hsu, R. Lau, B. P. Bowen, S. Hromada, T. Northen, and A. P. Arkin, *Molecular systems biology* **14** (2018).
- [16] M. Fan, K. Wang, and D. Jiang, *Mathematical Biosciences* **160**, 47 (1999).
- [17] J. A. Vano, J. C. Wildenberg, M. B. Anderson, J. K. Noel, and J. C. Sprott, *Nonlinearity* **19**, 2391 (2006).
- [18] R. M. May, *Nature* **238**, 413 (1972).
- [19] S. Allesina and S. Tang, *Nature* **483**, 205 (2012).
- [20] T. Gibbs, J. Grilli, T. Rogers, and S. Allesina, *Phys. Rev. E* **98**, 022410 (2018).
- [21] L.-Z. Wang, R.-Q. Su, Z.-G. Huang, X. Wang, W.-X. Wang, C. Grebogi, and Y.-C. Lai, *Nature Communications* **7**, 11323 (2016).
- [22] D. Merenstein, N. El-Nachef, and S. V. Lynch, *Journal of Pediatric Gastroenterology and Nutrition* **59** (2014).
- [23] T. S. Rayner and R. G. Creese, *New Zealand Journal of Marine and Freshwater Research* **40**, 477 (2006).
- [24] T. Scotti, M. Mimura, and J. Y. Wakano, *Ecological Complexity* **21**, 157 (2015).
- [25] S. J. Whipple, J. S. Link, L. P. Garrison, and M. J. Fogarty, *Fish and Fisheries* **1**, 22 (2000).
- [26] A. L. Hartman, D. M. Lough, D. K. Barupal, O. Fiehn, T. Fishbein, M. Zaslhoff, and J. A. Eisen, *Proceedings of the National Academy of Sciences* **106**, 17187 (2009).
- [27] C. De Filippo, D. Cavalieri, M. Di Paola, M. Ramazzotti, J. B. Poullet, S. Massart, S. Collini, G. Pieraccini, and P. Lionetti, *Proceedings of the National Academy of Sciences* **107**, 14691 (2010).
- [28] S. Jalili-Firoozinezhad, F. S. Gazzaniga, E. L. Calamari, D. M. Camacho, C. W. Fadel, A. Bein, B. Swenor, B. Nestor, M. J. Cronce, A. Tovagliari, O. Levy, K. E. Gregory, D. T. Breault, J. M. S. Cabral, D. L. Kasper, R. Novak, and D. E. Ingber, *Nature Biomedical Engineering* **3**, 520 (2019).
- [29] K.-H. Lin, B.-Y. Liao, H.-W. Chang, S.-W. Huang, T.-Y. Chang, C.-Y. Yang, Y.-B. Wang, Y.-T. K. Lin, Y.-W. Wu, S.-L. Tang, and H.-T. Yu, *BMC Genomics* **16**, 1029 (2015).